

## Validation of the seismic response of an RC frame building with masonry infill walls - The case of the 2017 Mexico earthquake

Tania C. Albornoz<sup>1</sup>, Leonardo M. Massone<sup>\*1</sup>, Julian Carrillo<sup>2</sup>,  
Francisco Hernández<sup>1</sup> and Yolanda Alberto<sup>1</sup>

<sup>1</sup>*Department of Civil Engineering, University of Chile, Blanco Encalada 2002, Santiago, Chile*

<sup>2</sup>*Universidad Militar Nueva Granada, UMNG, Cra. 11, Bogotá, Colombia*

(Received August 21, 2021, Revised January 27, 2022, Accepted March 8, 2022)

**Abstract.** In 2017, an intraplate earthquake of Mw 7.1 occurred 120 km from Mexico City (CDMX). Most collapsed structural buildings stroked by the earthquake were flat slab systems joined to reinforced concrete (RC) columns, unreinforced masonry, confined masonry, and dual systems. This article presents the simulated response of an actual six-story RC frame building with masonry infill walls that did not collapse during the 2017 earthquake. It has a structural system similar to that of many of the collapsed buildings and is located in a high seismic amplification zone. Five 3D numerical models were used in the study to model the seismic response of the building. The building dynamic properties were identified using an ambient vibration test (AVT), enabling validation of the building's finite element models. Several assumptions were made to calibrate the numerical model to the properties identified from the AVT, such as the presence of adjacent buildings, variations in masonry properties, soil-foundation-structure interaction, and the contribution of non-structural elements. The results showed that the infill masonry wall would act as a compression strut and crack along the transverse direction because the shear stresses in the original model (0.85 MPa) exceeded the shear strength (0.38 MPa). In compression, the strut presents lower stresses (3.42 MPa) well below its capacity (6.8 MPa). Although the non-structural elements were not considered to be part of the lateral resistant system, the results showed that these elements could contribute by resisting part of the base shear force, reaching a force of 82 kN.

**Keywords:** ambient vibration test; infill wall; masonry; Mexico earthquake; nonlinear model; RC frame

### 1. Introduction

Mexico City is in an area of significant seismic activity due to the action of five tectonic plates: the Caribbean, Pacific, North American, Rivera, and Cocos plates. The Cocos plate subducts below the North American plate at a convergence rate of 6 cm/year, and it generates recurrent earthquakes. On September 19, 2017, at 18:14:40 hours GMT (13:14:40 local time in central Mexico), an intermediate-depth normal-fault intraplate earthquake of magnitude Mw 7.1 occurred at a depth of 57 km with an epicenter between Puebla and Morelos, approximately 120 km from Mexico City (WGNSS 2017). The peak ground acceleration (PGA) of the seismic event was 0.2 g at the Lomas Estrella (LEAC) station in Iztapalapa, Mexico City, causing extensive building damage

---

\*Corresponding author, Professor, E-mail: lmassone@uchile.cl



Fig. 1 Observed damage on (a) and (b)

and numerous collapses. The recorded PGA exceeds by 30% the PGA measured at the Secretary of Communications and Transport (SCT) station (Galvis *et al.* 2020).

Since Mexico City is founded on the beds of ancient lakes Xochimilco and Texcoco, the soil below the city has varied characteristics and properties. As a result, the CDMX seismic code (PAFD 2004) prescribes a detailed seismic microzonation system, because the natural period and deposit depth of soft clay deposits vary significantly along the CDMX basin (with Vs30 values ranging from 60 to 70 m/s). CDMX seismic code includes three main zones, where Zone I, known as the hill zone, is characterized by a firm soil, mainly rock formations, Zone II, known as a transition zone, is characterized by layers of sand and sandy silt alternating with layers of lacustrine clays and, finally, Zone III, known as lake zone, which is characterized by thick clay layers. In particular, the lake zone (Zone III) is subdivided into four sub-areas (IIIa, IIIb, IIIc and IIId), whose periods ranged between 1 s and 1.5 s for Zone IIIa, 1.5 s and 2.5 s for IIIb, 2.5 s and 3.5 s for IIIc, and period values greater than 3.5 for Zone IIId which is based on a clay deposit with a depth ranging from 20 to 50 meters. Ochoa-Cornejo *et al.* (2019) reported that Zones IIIa and IIIb of CDMX experienced the most significant damage in 2017; this zone concentrates structures with less than 10 stories. In fact, the building collapses were highly influenced by the double resonance phenomena, which occur when a building's natural period is similar to that of the soil deposit. The type of soil with such a property corresponds to lake deposits that are generally covered with artificial fill and alluvial soils. Highly compressible plastic clays are found in this zone, interspersed with sand layers with clay and silt content. This zone is characterized by a high-water content that contributes to the amplification of seismic waves.

During the Mw 7.1 earthquake in Mexico City, 44 buildings located in Zones IIIa and IIIb collapsed, with most of the buildings (~40%) in the range of 5 to 6 stories (Galvis *et al.* 2020), 360 buildings needed to be demolished or retrofitted, and a total of 1136 buildings needed repair (CIRES 2017). A significant number of buildings that collapsed during the 2017 earthquake had a soft first story (used for parking spaces), as shown in Fig. 1(a) (Galvis *et al.* 2020, Reinoso *et al.* 2021, Lan *et al.* 2020). This system provides low lateral stiffness, because the infill masonry walls that resist the earthquake demands are absent in the first story.

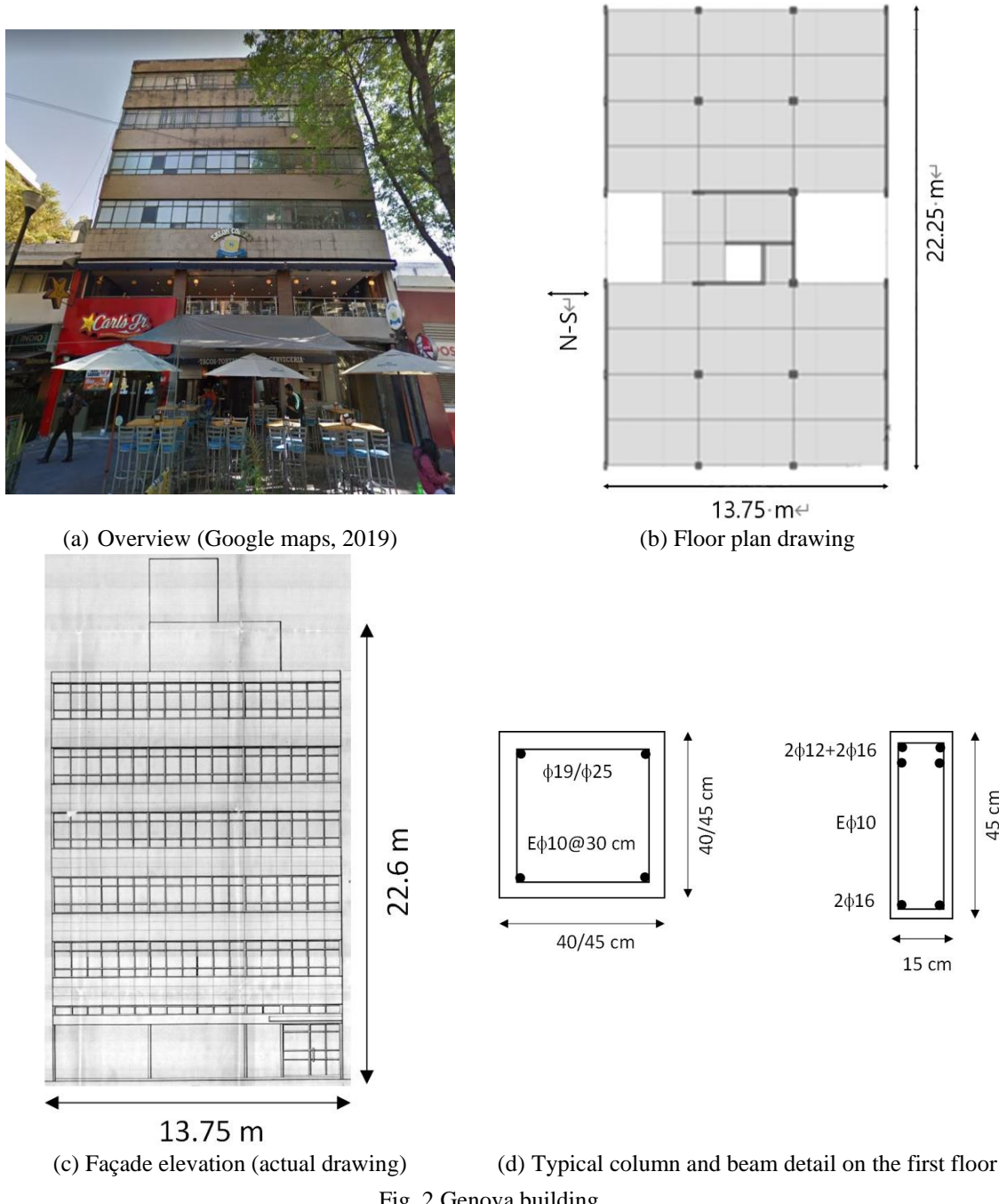
In addition to the soft-first-story mechanism, many buildings are structured with flat slab systems that do not include beams connected to columns (i.e., it is not a seismic frame), meaning that the system depends on the slab-column interactions. This results in low stiffness systems, reduced structural ductility, and significant negative moments in the slabs, where small changes in demand may lead to large changes in the response (Alcocer *et al.* 2020). In addition, in some cases, the stirrup spacings were excessive in critical zones, and thus shear forces were not fully resisted, or ductility was significantly limited (Fig. 1(b)). Moreover, the lack of confinement steel around the concrete cores of columns reduced structural ductility, leading to concrete crushing and the buckling of longitudinal reinforcing bars (Galvis *et al.* 2017). Most of the building collapses observed during the 2017 earthquake occurred in buildings located on corners. The façades facing the street had no infills, and the perimeter walls opposite the road had masonry walls, generating eccentricities and torsional effects in the structure. In addition, damage to corner buildings increased due to pounding with neighboring structures given the seismic movement and the limited or nonexistent separation between buildings (Gómez *et al.* 2019). Most of the buildings which collapsed were those with flat slab systems and RC columns. The lowest number of collapsed buildings were those with RC walls (Galvis *et al.* 2017).

Previous studies have modeled buildings that were damaged by earthquake demands, providing element formulation and the modeling assumptions that were required to capture a specific failure mode (e.g., Arteta *et al.* 2019, Massone *et al.* 2021, Lemnitzer *et al.* 2014), and others have used simple approaches to correlate displacement demands and damage levels (e.g., Massone and Cáceres 2020). However, there is minimal literature dealing with buildings without damage but with similar configurations to those that were damaged, in order to understand the impact of different modeling assumptions. This work assesses the response of a building in Mexico City that was not damaged structurally, despite having a configuration similar to those of damaged buildings. The analysis considers different modeling assumptions for the construction of nonlinear models. This approach seeks to address different issues that structural engineers face in the selection of elements or modeling considerations, such as membrane or strut models for masonry, the effect of soil-structure interaction, interaction with neighboring buildings, the impact of partitions on stiffness, and the strength of frame buildings with infills. Five 3D numerical models were used in the study to model the seismic response of the building and to identify key aspects that are relevant to predict a reliable response for RC frame systems with masonry infill walls. The building dynamic properties were identified using an ambient vibration test (AVT), enabling validation of the building's finite element models. Although the model selection does not provide several options for element formulation, after reviewing the different alternatives, the results for this building model are shown to be consistent with the absence of damage. The results aid in explaining why the actual building withstood the earthquake despite presenting the same characteristics as damaged and/or collapsed buildings.

## 2. Case study

### 2.1 General description

The building under study is located at 70 Genova Street in Mexico City, at  $19.425^\circ$  latitude and  $-99.163^\circ$  longitude. Fig. 2(a) shows the front view of the building from the main street. The



corresponding seismic zone is IIIb, according to the Mexico City Standards for Seismic Design (PAFD 2004). The building was built in 1954, using the recommendations prescribed by the Construction Standards of 1942, which considers a seismic coefficient of 0.025 (Federal District Department 1942). To date, the building has withstood three strong earthquakes, in 1957 (Mw 7.8),

1985 (Mw 8.1), and 2017 (Mw 7.1). Overall, it has sustained minor damage to the exterior facades because of pounding from the neighboring two-story buildings. The building is an RC frame system in the longitudinal and transverse directions, with masonry concrete block infill walls on the facades, stairs, and elevator shaft.

## 2.2 Structural system and model considerations

The structure is a six-story building with a height of 19.51 m to the top of the sixth story. There is a small service room on top of the building, giving a total building height of 22.60 m (Fig. 2(c)). The first-floor height (S1) is 3.76 m, and the height of each of the upper stories is 3.15 m. The RC frame system includes four columns in the north-south (transverse) direction, spaced at 4.55 m, 4.65 m, and 4.55 m, respectively, as shown in Fig. 2(b). In the longitudinal direction, there are six columns with a spacing of 4.45 m and joined by beams. The frame beams extend in both directions. Half-span beams are placed in the north-south (transverse) direction (Fig. 2(b)). This configuration generates a plan of 13.75 m by 22.25 m. The columns size varies from level to level and also across the floor plan, however, on the first floor (S1) the column width varies from 25 cm to 65 cm, whereas commonly interior columns are either 40 cm by 40 cm or 45 cm by 45 cm, with an equivalent average column width of 40.5 cm ( $\sqrt{\text{Area}_{\text{column}}}$ ). Longitudinal reinforcement is commonly 4-f19mm or 4-f25mm, with stirrups f6mm or f10mm spaced at 30 cm (Fig. 2(d)). Beam dimensions vary less than columns, where the width is always 15 cm, except for the interior beams in the longitudinal direction (E-W), which are increased to 20 cm. The height of the beams is 45 cm for all axis (Fig. 2(d)), except for an interior short beam (elevator shaft) which is 30 cm. Reinforcement details also vary in different sections, but on the first floor, several sections present 2f12+2f16 at beam top and 2f16 at beam bottom as longitudinal reinforcement, and stirrups f10mm with variable separations from 10 cm to 50 cm. Beams connect the vertical elements of the lateral resistance system in both directions and support a 10-centimeter-thick RC slab. The slab is modeled as a rigid diaphragm, but out-of-plane flexibility (elastic) is considered.

Only one block masonry wall is fully confined in the transverse direction; the other transverse walls are not adequately confined around their perimeters (Fig. 2(b)). In the longitudinal direction, the masonry concrete block infill walls (comprised of 40 cm x 20 cm x 15 cm blocks) contact the structural RC frames; therefore, they are load-bearing infill walls acting with the surrounding concrete structure. These walls are 15 cm thick, providing stiffness to the system in the east-west direction. Therefore, the structural system can be described as an RC frame with unreinforced masonry infills. Masonry infill walls are a cheap alternative to reinforced concrete walls, since they add stiffness and resistance to the structural system if they are correctly attached to the frame that confines them; if not, the story drifts and the period of the building would increase (Pujol and Rodriguez 2017).

The structural analysis was carried out using the ETABS computer program (CSI 2014). Table 1 shows the nominal properties of the materials used in the design and construction of the building: concrete (Mendoza 1985), masonry (Meli and Reyes 1971), and steel reinforcement (Rodríguez and Botero 1996). The uniaxial stress-strain curves for masonry, concrete, and steel are shown in Figs 3(a) and 3(b), respectively.

The model formulation includes a mesh of 1 m x 1 m elastic shell-type elements for masonry walls (Models A and B - see Section 3) and longitudinal elements with plastic hinges at a relative distance of 0.05 and 0.95 of the element lengths for beams and columns, giving rise to a concentrated plasticity mechanism after yielding to characterize their nonlinear response. The defined hinges are

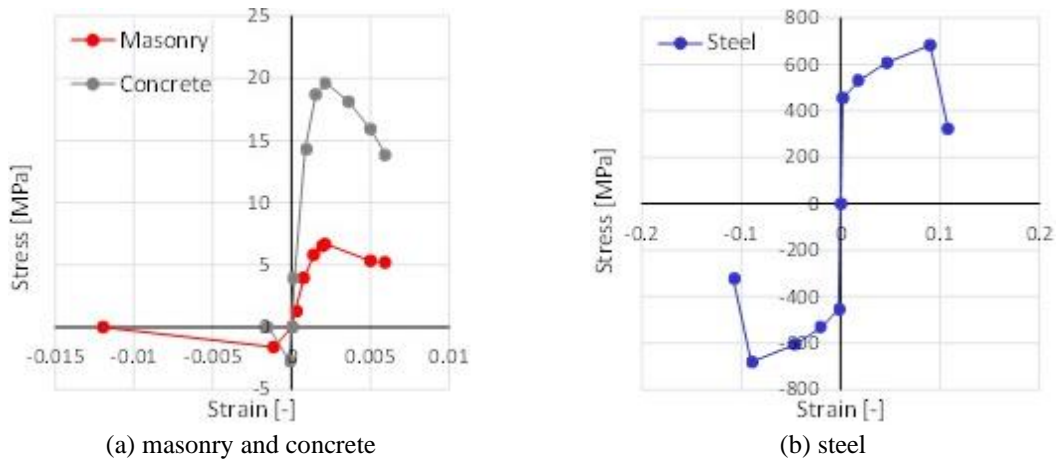


Fig. 3 Stress-strain curves

Table 1 Material properties

Mechanical property	Concrete (Mendoza 1985)	Masonry (Meli and Reyes 1971)	Steel reinforcement (Rodríguez and Botero 1996)
Unit weight [ $kN/m^3$ ]	23.5	21.2	76.9
Modulus of elasticity [MPa]	$2.1 \times 10^4$	$1.5 \times 10^3$	$2 \times 10^5$
Poisson ratio	0.18	0.2	-
Shear modulus [MPa]	$8.9 \times 10^3$	610	-
Strength [MPa]	20 ( $f'_c$ )	6.7 ( $f'_m$ )	420 ( $f_y$ )

of the fiber type, where each fiber represents a tributary area of concrete and steel, to characterize flexural behavior. For simplicity, shear failure is not assessed in the model, given that such damage type was not observed. Therefore, shear stresses must be analyzed independently to determine if the demanding stresses exceed the shear capacity. Infill wall panels in RC frame buildings act as diagonal struts under large seismic actions, rather than acting as wall panels (Tabeshpour and Arasteh 2019, Bouarroudj and Boudaoud 2022). Gaps between the masonry infill and the RC frame drastically minimize the capability of infill walls to resist lateral forces in a seismic event. These gaps may already exist before an earthquake due to construction tolerances (EERI 2011). To represent this behavior, an alternative model for masonry was considered based on struts (Models C, D and E - see Section 3). In this work, the area of the diagonal strut is defined as the width,  $b_s$ , multiplied by  $a_w = (0.25 + 0.85 N/A_w f'_m) l_w$ , where  $A_w$  ( $0.77 \text{ m}^2$ ) is the net area of the masonry section,  $l_w$  ( $5.1 \text{ m}$ ) is the length of the section in the direction of the shear force,  $f'_m$  ( $6.7 \text{ MPa}$ ) is the compressive strength of the masonry, and  $N$  ( $246 \text{ kN}$ ) is the vertical force (Hwang 2001). Then, to carry out the modeling, struts with an area equivalent to the strut in compression are considered in each diagonal direction. Table 2 summarizes the distribution of the walls along with the height ( $h$ ) of the structure. The area of the unreinforced masonry infill walls in the longitudinal direction ( $A_{w_l}$ ) is approximately four times larger than that in the transverse direction ( $A_{w_t}$ , short direction). For the study building, the masonry wall density (the ratio between the area of the walls in one direction and the total plan area,  $A_f$ ) is 3.1% in the longitudinal direction ( $x$ )

Table 2 Distribution and weight of masonry infill walls along the height of the building

Floor	$h$ [m]	$A_f$ [ $m^2$ ]	$A_{w_l}$ [ $m^2$ ]	$A_{w_t}$ [ $m^2$ ]	Weight [kN]
S1	3.76	302.3	9.47	2.53	16080
S2 to S5	3.15	269.6	6.30	1.67	36150*
Rooftop	3.15	269.6	6.30	1.67	2891
Service Room	3.15	28.5	1.63	1.67	462.9

\*Including the total of the S2 to S5 floors

Table 3 Mean values of steel ratios in columns and beams

Floor	Columns		Beams		
	$\rho$ Long. [%]	$\rho$ Transv. [%]	$\rho$ Long. Top [%]	$\rho$ Long. Bot. [%]	$\rho$ Transv. [%]
S1	0.80	0.09	1.12	0.87	0.58
S2	1.23	0.18	1.12	0.87	0.58
S3 to S4	1.11	0.11	1.00	0.78	0.58
S5	0.96	0.12	1.00	0.78	0.58
Rooftop	0.96	0.15	1.05	0.85	0.66

and 0.8% in the transverse direction (y) at the ground floor level. The wall density of the building is low, particularly in the transverse direction, compared with confined masonry buildings in high seismic hazard zones (Astroza *et al.* 2012). Table 3 shows the mean values of the steel ratio of longitudinal ( $\rho$  Long.) and transverse ( $\rho$  Transv.) reinforcement for the columns and beams of the Genova building.

Although not all the characteristics that were observed in buildings with damage were present in the case study building, several relevant aspects can be mentioned: (1) the number of stories (6) with a flexible structural system in one direction implies that displacement demands are similar to other damaged structures, especially since the location is close to buildings with severe damage, (2) unreinforced masonry as infill in selected locations, which locally increases the stiffness, (3) columns with low transverse reinforcement (Table 3) where the transverse steel ratio is about 0.1%, whereas the minimum steel quantity according to ACI 318-19 is close to 1% (volume) for columns from special moment frames, and (d) neighboring buildings that cause pounding at the second level.

### 2.3 Acting loads

The permanent live load for residential buildings such as apartments, houses, and hotel rooms prescribed by state construction regulations (Federal District Department 1942) is equal to 1.5 kN/m<sup>2</sup>. A modal analysis was performed, considering the self-weight and 100% of the live load. Table 2 shows the values of the weight per story for the seismic analysis, which includes the foundation beams.

### 2.4 Ambient vibration tests (AVT)

One of the objectives of the work is to provide a reliable model for the building. The period of

Table 4 Test configuration

Test	Recorder		
	R1	R2	R3
1	1	4	5
2	1	2	3
3	1	6	3
4	1	7	8

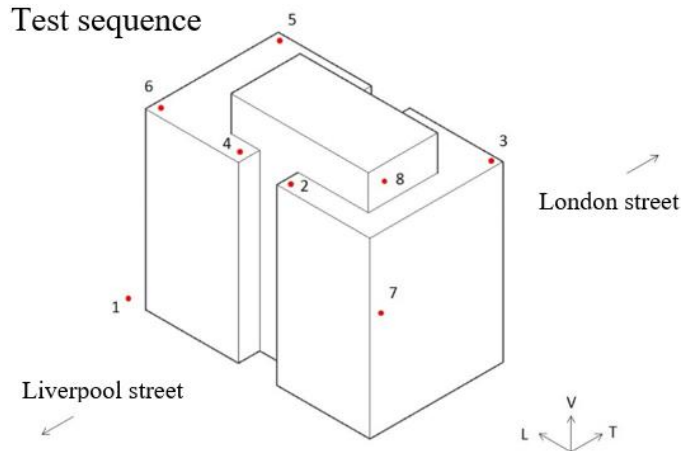


Fig. 4 Location of the sensors for AVT

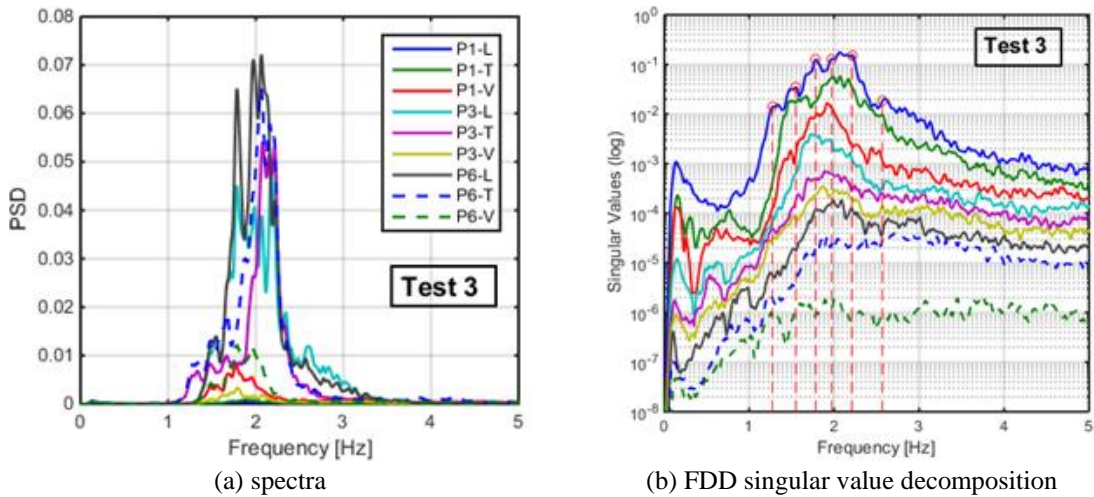


Fig. 5 Power spectral density

the structure, besides the presence or not of damage, are the only parameters that can be used to verify model assumptions. Thus, four ambient vibration tests (AVTs) were carried out in the Genova building by Guerrero (2018). AVTs were performed considering different sensor configurations using three triaxial accelerometer-type sensors (R1, R2 and R3), as shown in Table 4.

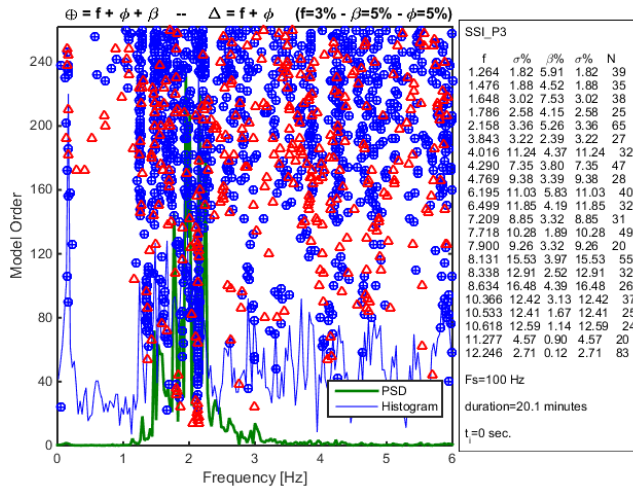


Fig. 6 Stability diagram. From SSI and Test 3

Table 5 Identified natural frequencies

Mode	FDD (Hz)	SSI (Hz)
1 Tr-To	1.272	1.264
2 Lo	1.548	1.476
3 Lo-To	*	1.648
4 Lo-To	1.782	1.786
5 To-Lo	1.972	**
6 To	2.208	2.158
7 Lo-To	2.566	**
8 Tr-To	***	3.843

\*It can be observed in FDD SV; however, it cannot be identified clearly.

\*\* It cannot be marked clearly with SSI because of mode mixing and the small number of sensors

\*\*\* small energy, it cannot be observed clearly with FDD

Each AVT was performed for 20 minutes, and synchronized records were obtained at a sampling rate of 100 sps. The accelerometers were in different locations (1-8), as shown in Fig. 4, where L, T, and V correspond to the longitudinal, transverse, and vertical directions.

Three system identification techniques were used in this study to estimate the dynamic properties of the building (natural frequencies, damping ratios, and mode shapes) from the AVTs: i) Frequency analysis (PSD or power spectral density, coherence, and transfer function) (Bendat and Piersol 2011); ii) FDD (frequency domain decomposition) (Brincker *et al.* 2001); and iii) SSI (subspace system identification) (Van Overschee and De Moor 1996). The last two techniques allow for disaggregating mode shapes related to close frequency values. Fig. 5(a) shows the PSD using the Welch method obtained from each sensor recorded during Test 3. The results shown in Fig. 5(b) indicate that the structure has multiple modes between 1.2 and 2.6 Hz (~ 7 modes). The SSI method obtains the dynamic properties of the structure by assuming linear behavior. This methodology can disaggregate modes if sensors are placed at multiple levels (Van Overschee and

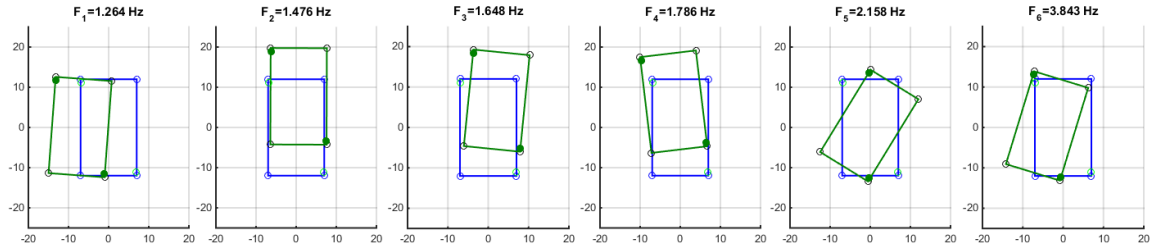


Fig. 7 Modal shapes in plan-view of Genova building

Table 6 Soil properties (Jaime et al. 1987)

Soil Type	Thickness [m]	N	$\gamma$ [kN/m <sup>3</sup> ]	Vs [m/s]	G [kN/m <sup>2</sup> ]	$\nu$
Filling	1.2	35.3	18.6	100.0	18990	0.49
Gray clay	4.8	3.0	14.0	97.1	15794	0.49
Greenish brown clay with sand lens	3.0	2.6	12.9	49.0	3615	0.49
Greenish clay	1.2	1.5	11.5	33.5	1337	0.49
Greenish brown clay	2.1	1.5	11.3	44.3	2289	0.49
Greenish brown clay with sand	1.8	7.0	11.3	54.3	3527	0.49
Greenish clay with not much sand	2.7	4.0	15.2	62.5	5130	0.49
Fine sand with clay	1.2	3.5	16.2	46.5	2632	0.49
Greenish brown clay with sand lens	0.6	2.0	11.6	50.0	2964	0.49
Dark gray fine sand	0.6	12.0	16.7	55.0	3439	0.49
Greenish brown clay	0.9	1.0	12.3	63.0	4770	0.49
Firm Ground	30	-	17.7	386.7	-	-

De Moor 1996). Fig. 6 shows the stability diagram obtained from the SSI method. The system dynamic properties are obtained from discrete state-space matrices estimated directly from AVT data, assuming that the structure is described by a linear elastic system related to increasing order values (from 2 to 260). The dynamic properties can be obtained independently for each order of the discrete space-state system. However, these properties can change between systems of different orders. Therefore, the most reliable dynamic properties are those that are most frequently observed between systems of different order values. The blue circles refer to three coincidences (frequency, modal shape and damping ratio). The red triangles refer to double coincidence (frequency and mode shape). Similitude criteria are employed to compare the dynamic properties estimated from the space-state discrete system of consecutive orders. Fig. 6 also includes the average PSD of the recorded channels and the histogram that accounts for the coincidences for each frequency found for different order values. In addition, Fig. 6 is accompanied by a table indicating the number of matches (N) and the standard deviation of the identified parameters. Table 5 summarizes the natural frequencies identified using the FDD and SSI techniques for Test 3. Similar results were obtained with both methods, displaying similar mode shapes. However, it was challenging to uncouple the modes of close frequencies because of the small number of sensors employed during the AVTs.

Fig. 7 shows the first modal shapes for the Genova building obtained using the FDD method

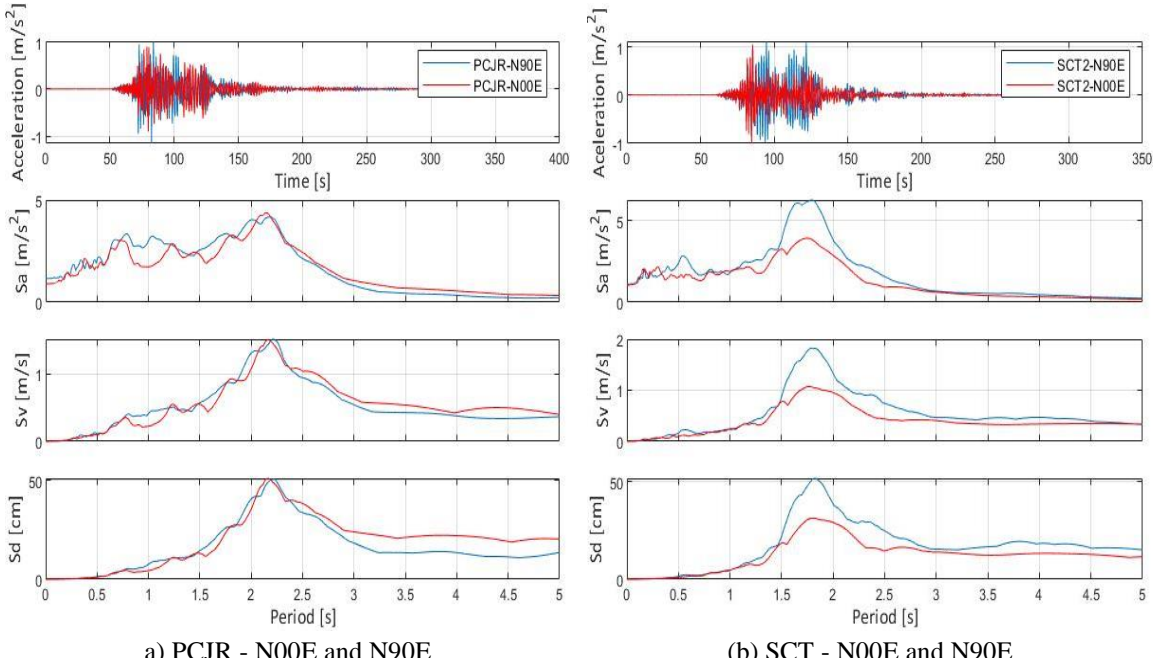


Fig. 8 Acceleration records and response spectra

(similar to SSI) for Test 3. The figure shows that the first and second vibration modes are associated with the transverse and longitudinal directions, with associated periods of vibration of 0.791 s ( $f = 1.264$  Hz) and 0.678 s ( $f = 1.476$  Hz), respectively. The torsional mode is associated with Mode Shape 5, and the corresponding period of vibration is 0.463 s ( $f = 2.158$  Hz).

## 2.5 Soil characteristics

According to the CDMX seismic code (Federal District Government 2004), the Genova building is located in Seismic Zone IIIb. Based on the same document, the natural period of the soil deposit is 2.1 s, and the total thickness of the soft soil is approximately 32 m. Table 6 summarizes the soil properties reported at the Secretary of Communications and Transport (SCT) station (Jaime *et al.* 1987), a seismic station in Zone IIIb with a natural soil period of 2.0 s.

Table 6 shows the thickness of each soil layer, the number of blows from the Standard Penetration Test (SPT N), volumetric weight ( $\gamma$ ), Poisson's ratio ( $\nu$ ), and some dynamic properties, such as the shear modulus and shear wave velocity. The equation  $G = V_s^2 \rho$  was used to estimate the shear modulus (G) for small soil deformations, where  $V_s$  [m/s] is the shear wave velocity and  $\rho$  ( $kg/m^3$ ) is the soil density. These properties were assumed to be similar at the Genova building location. This allows for estimating the soil parameters needed to compute the site response using the one-dimensional analysis detailed in Section 2.7 and estimating the equivalent dashpots and springs to model the soil-foundation-structure interaction (SFSI, Section 2.8). Dashpot and spring (longitudinal and rotational) elements were added to the model with the properties detailed in Section 2.8 (Table 7). In the case of springs, elastic behavior was considered and in the case of dashpots, viscous damping was added.

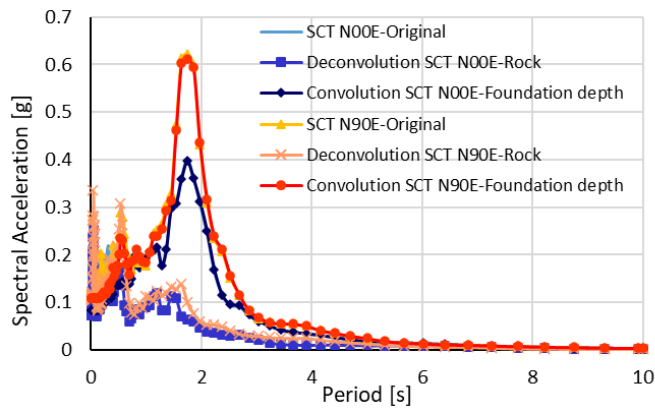


Fig. 9 Response of the SCT - N00E and SCT - N90E records at different soil profiles

## 2.6 Seismic records

Two seismic records from the Puebla-Morelos 2017 earthquake were selected because they were recorded in the same seismic zone as the Genova building (Seismic Zone IIIb). Thus, they are related to a natural soil deposit with a natural frequency similar to that found at the building's location (~ 2 sec) (Federal District Government 2004). The PCJR is one of the closest stations, only 700 m from the Genova building. The SCT station is located farther away (4.16 km), but more severe damage and building collapses were observed near this station. Also, the soil deposit depth is 30 m for the PCJR station and 40 m for the SCT station. The natural period of the soil deposit at the Genova building is 2.1 s and the soil deposit depth is 32 m.

Fig. 8 shows the acceleration records and the acceleration, velocity, and displacement spectra in each direction for the PCJR and SCT stations for a damping ratio of 5%. The peak spectrum values were 2.2 sec for PCJR and 1.8 sec for SCT. Other stations are either far from the location of the building or over a different soil type. Given that the intention is to provide a reliable response of the building to the observed earthquake, analysis with the selected records was considered appropriate.

The spectrum values related to the principal natural periods of the Genova building (0.46-0.79 sec) are not close to the peak acceleration spectrum values (0.15-0.30 g); that is, the building period does not coincide with the natural period of the soil.

## 2.7 Soil response at the Genova building site

A one-dimensional analysis of the local site response for the SCT record location was performed using the software DEEPSOIL V6.1 (Hashash 2016). This analysis considered the site's actual deposit depth and the seismic response experienced at the foundation level (1 meter depth). A linear elastic analysis in the frequency domain was performed by assuming a constant damping ratio of 5%. In this context, the seismic record is deconvoluted to obtain the bedrock excitation (within the signal). Then, the excitation signal is processed assuming the same stratigraphy of the SCT site (Table 6), but with the deposit depth reduced to 32 m to eliminate the lower soil layers. Finally, the soil layer seismic response at the foundation level is taken as the structure input ground motion. Fig. 9 shows the deconvolution and convolution process applied to the SCT

Table 7 Stiffness and damping obtained for the Genova building

Stiffness			Damping		
Direction	Study building	SCT	Direction	Study building	SCT
$k_z \left[ \frac{kN}{mm} \right]$	529	910	$C_z \left[ kN \frac{s}{mm} \right]$	54.4	93.7
$k_y \left[ \frac{kN}{mm} \right]$	417	718	$C_y \left[ kN \frac{s}{mm} \right]$	30.5	52.6
$k_x \left[ \frac{kN}{mm} \right]$	400	688	$C_x \left[ kN \frac{s}{mm} \right]$	28.40	49
$k_{zz} \left[ kN \frac{mm}{rad} \right]$	$4.66 \times 10^{10}$	$8.02 \times 10^{10}$	$C_{zz} \left[ kN - mm \frac{s}{rad} \right]$	$9.02 \times 10^8$	$1.56 \times 10^9$
$k_{yy} \left[ kN \frac{mm}{rad} \right]$	$4.79 \times 10^{10}$	$8.25 \times 10^{10}$	$C_{yy} \left[ kN - mm \frac{s}{rad} \right]$	$7.28 \times 10^8$	$1.26 \times 10^9$
$k_{xx} \left[ kN \frac{mm}{rad} \right]$	$2.63 \times 10^{10}$	$4.53 \times 10^{10}$	$C_{xx} \left[ kN - mm \frac{s}{rad} \right]$	$2.96 \times 10^4$	$5.10 \times 10^8$

seismic record for its components. From this, the seismic response obtained for the base of the foundation is slightly higher than the original one. The response obtained is then used for the analysis that considered the soil-structure interaction.

### 2.8 Soil-foundation-structure interaction (SFSI)

The values of equivalent stiffness ( $k_i$ ) and dashpot ( $C_i$ ) for the horizontal, vertical, and rocking movements were obtained from the equations suggested by Pais and Kausel (NEHRP 2012). These equations consider a shallow foundation with a rigid rectangular shape and a uniform horizontal soil half-span. These values are described along the axes ( $x$  = longitudinal,  $y$  = transverse, and  $z$  = vertical) and around the axes ( $xx$ ,  $yy$ , and  $zz$ ) (NEHRP 2012). To calculate these parameters, it is assumed that the foundation vibrates according to the fundamental natural period of the structure in each direction. On the other hand, the volumetric weight ( $\gamma$ ), the soil period ( $T_s$ ), and the depth of the firm soil profile ( $H_s$ ) are considered to calculate the shear modulus  $G = (H_s/T_s)^2 16\gamma/g$  (Federal District Government 2004) for the Genova building and the SCT station. Table 7 lists the results of soil stiffness and damping for the location of the Genova building and the SCT station. The table shows that the computed values are approximately twice those in the location of the study building; this may be because several of the building data were extrapolated from the SCT parameters. For this reason, the SCT record was used to perform the analysis.

## 3. Results and discussion

The seismic response of the building obtained from different numerical models is presented in this section. The analysis considered the geometry, reinforcement, material properties, loadings, and soil properties described in Sections 2.1 to 2.8. The seismic records used in the analysis were corrected for possible external interferences, such as environmental noise or disturbances in the accelerometers, using filters to eliminate high and low frequencies with a low pass filter of 8th order with a frequency of 0.1 Hz and a high pass filter of 4th order with a frequency of 30 Hz, both of the Butterworth type.

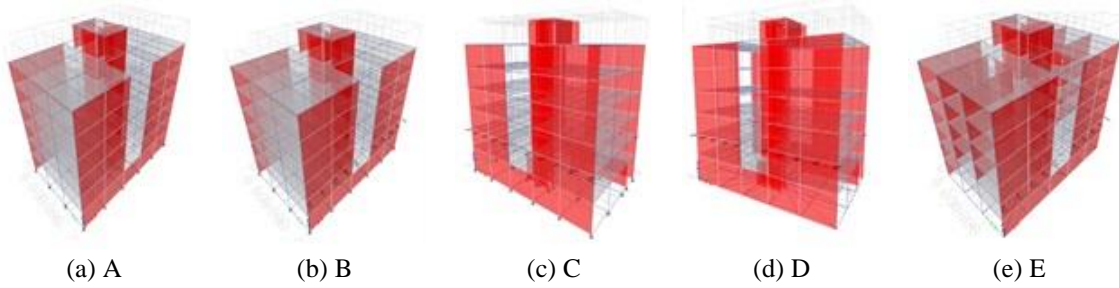


Fig. 10 Scheme of numerical models of the building

Table 8 Periods measured from AVTs and obtained from numerical analysis

Mode (Direction) / Period [s]	AVT	Model A	Model B	Model C	Model D	Model E
Description		Original model	Model A + neighboring buildings.	Model B + strut (axis 3), and reduced stiffness (axes 4 and 4a)	Model C + soil-structure interaction	Model D + masonry partitions
1 Transverse	0.79	0.86	0.71	0.97	0.96	0.87
2 Longitudinal	0.68	0.43	0.42	0.43	0.59	0.58
3 Torsional	0.46	0.52	0.46	0.46	0.44	0.44

Five 3D numerical models were used in the study to model the seismic response of the building. Model A, or the base model, treats all the walls as fiber shell elements. The building is fully fixed at the base, and interactions with adjacent buildings are ignored. Model A is used to perform the seismic response of the building subjected to the PCJR and SCT records. The results related to other configurations are presented for the SCT seismic record only, due to slight differences in the results. Model A is used in this study as a benchmark against which to analyze the results obtained for Models B to E, to which modifications are included (Fig. 10). Model B is based on Model A and considers the effect of the adjacent buildings using lateral springs at the level of the second floor. Model C is based on Model B and simulates the masonry walls using compression struts instead of shell elements, including allowances for cracking and stiffness degradation. Model D is based on Model C and incorporates soil-foundation-structure interaction (SFSI) by adding springs and dashpots connecting the foundation to the soil. Model E is based on Model D and ensures that the stiffness and strength contribution of the masonry infill walls are accounted for. Table 8 shows the transverse, longitudinal, and torsional natural periods of vibration measured from the AVTs and those obtained using the different configurations. The results from Models A to E demonstrate progressive improvement in the estimation of the natural periods of vibration associated with the three fundamental modal shapes compared with the results from the AVTs. In particular, the incorporation of SFSI improves the natural frequency estimation of the system, since AVT measurement also includes the interaction of the structure with the soil.

### 3.1 Model A: Original model

Fig. 10(a) shows a schematic of the 3D numerical model A. Fig. 11(a) shows the ground floor

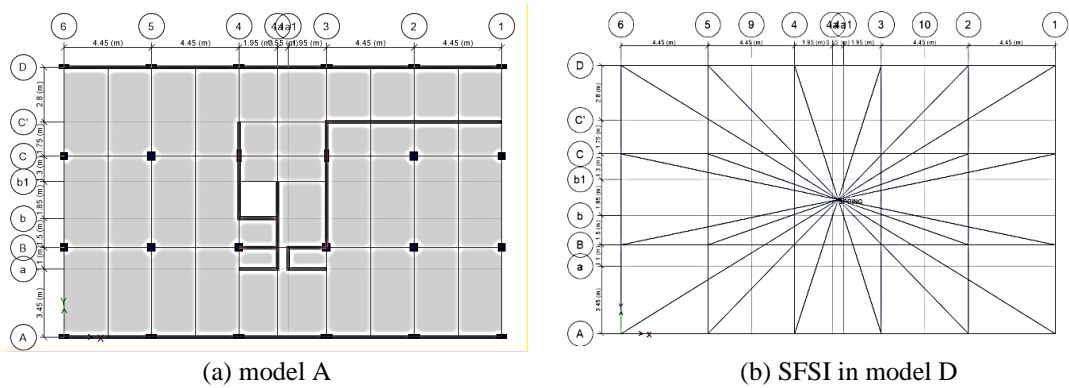


Fig. 11 Plan view of ground floor

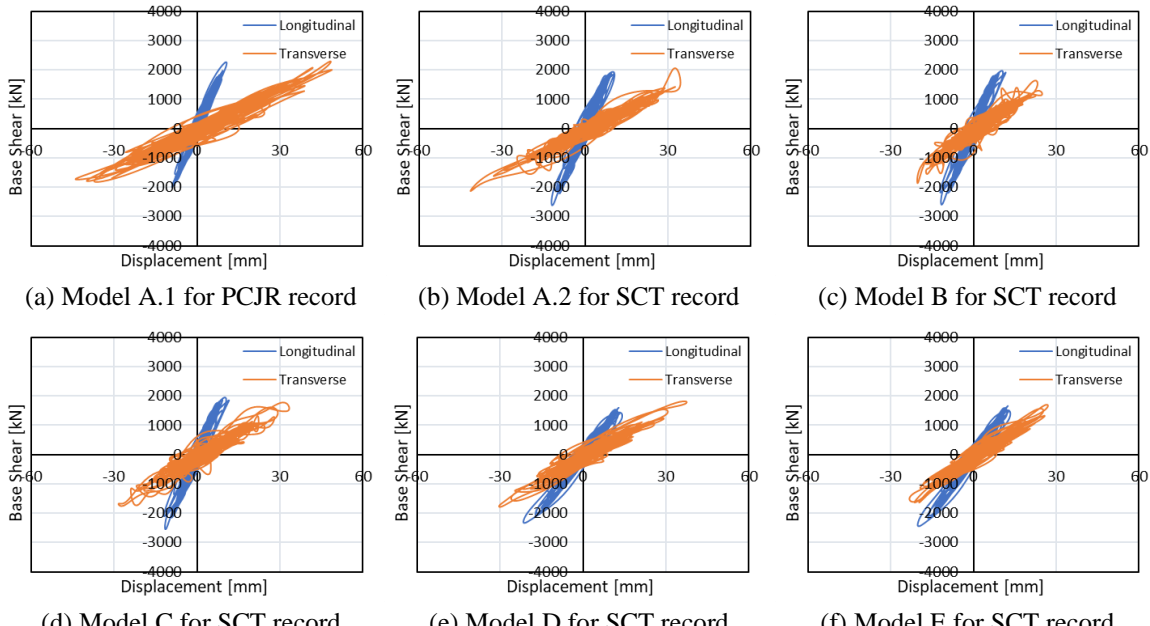


Fig. 12 Base shear versus roof displacement

of the building, highlighting the fact that the ground floor does not have slab openings and is bounded at that level by a continuous wall in the longitudinal direction. The ground floor also includes a wall located on Axis C', between Axes 1 and 3. In Fig. 11(a), the beams, columns, and walls are drawn in black, and the slabs in gray. As shown in Fig. 8(a), using the period of vibration in the transverse direction of the building (0.86 s, Table 8), the spectral acceleration for the PCJR record is  $1.85 \text{ m/s}^2$  in the same direction (N00E), and the corresponding value for the SCT record is  $1.71 \text{ m/s}^2$ .

### 3.1.1 Model A: Record of the PCJR station

Numerical analysis was carried out using the closest record to the building (PCJR, 700 meters away).

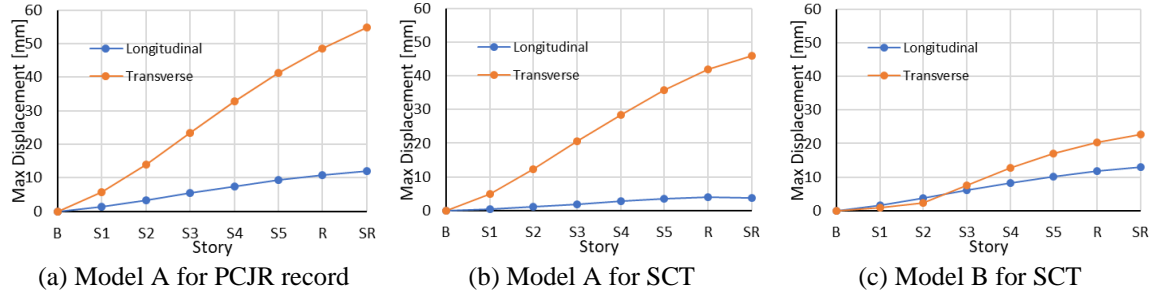


Fig. 13 Displacement shape of the building

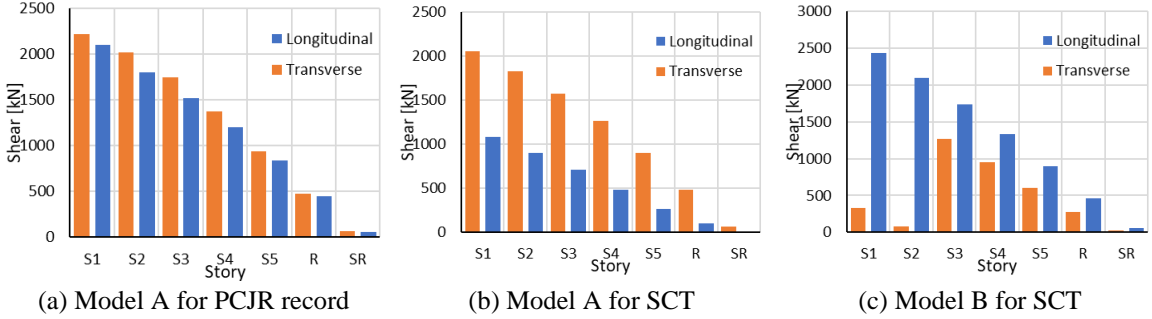


Fig. 14 Story shear of the building

It was expected that the model would not present significant damage because the building experienced only minor damage to its façade during the 2017 earthquake which was mainly associated with pounding against adjacent buildings. Fig. 12 shows the base shear force versus the displacement at the central point of the roof for each direction of the building. Fig. 12(a) shows that the response of Model A under the PCJR record is essentially linear in the longitudinal direction; however, it deforms considerably in the transverse direction.

Fig. 13 shows the maximum displacement of the center of mass of each floor. Fig. 13(a) shows that Model A experiences larger displacements in the transverse direction when using the PCJR record, reaching displacements at roof level of 55 mm (compared to 45 mm when the analysis is carried out using the SCT record). On the other hand, total displacements close to 10 mm are observed in the longitudinal direction.

Fig. 14 shows the inter-story shear forces in both directions at the time when the base shear reaches its peak value. As expected, Fig. 14 shows that the inter-story shear forces decrease as the height of the building increases, and their values in the transverse direction are slightly higher than those in the longitudinal direction for the PCJR seismic record. Plastic hinges are observed first in the columns located in the elevator shaft, caused by a bending moment. The peak shear force computed for the elevator wall is 879 kN (Axis 3), which is significantly higher than its shear stress capacity of 0.38 MPa, according to experimental data from Meli and Reyes (1971), which yields a shear strength of 265 kN; therefore, the shear force demand on the walls would be more than 2.4 times higher than their capacity. It should be mentioned that the model does not include shear failure, since the shell-type element considers non-linearity in bending only. The reduction in shear force in the second level of Model B (Fig. 14(c)) is explained by the constraint provided by adjacent buildings (see Section 3.2).

### 3.1.2 Model A.2 Record of SCT station

The SCT record was measured in the same seismic zone in which the building was built, and this seismic record refers to a zone where the most significant damage was observed during the 2017 earthquake. Fig. 13(b) shows that displacements in the longitudinal direction are smaller than those in the transverse direction because of the higher stiffness provided, which agrees with the displacements obtained from the spectra of the ground acceleration record. Fig. 12(b) also shows that the behavior of the building in both directions is mainly linear, and the transverse base shear is similar to the previous case (PCJR). As shown in Fig. 13(b), the deformation of the model is concentrated at the ground story along its flexible direction (transverse).

The story shear of Model A subjected to the SCT seismic record (Fig. 14(b)) evidenced the beginning of yielding in some columns in the transverse direction. Moreover, the shear force acting on the elevator wall is still much higher (813 kN) than its shear strength (265 kN), so that building collapse would be expected due to excessive shear stress. Thus, the numerical model using a shear-elastic shell-type element to model shear masonry walls would not be suitable to simulate the seismic behavior of the building, because the strength degradation of the elevator wall cannot be correctly addressed.

### 3.2 Model B: Model A + effect of adjacent buildings (Record of SCT station)

During the site inspection of the building, pounding damage was observed on the exterior longitudinal walls, particularly just above the second floor, which also coincides with the height of the surrounding buildings on both sides. Model B was modified to simulate this effect using elastic springs each with a stiffness constant of 30 kN/mm, which added to the stiffness of the building and resulted in achieving a period less than that measured during the AVT in the transverse direction of the building (see Table 8). Fig. 12(c) shows that the seismic behavior of the building is essentially linearly elastic, and the deformations have decreased compared to previous models.

Fig. 13(c) shows greater displacements at the third story level compared to lower stories, due to the fixity provided by the springs on the second floor. Even though damping helps to decrease the shear stresses at the first two stories (Fig. 14(c)), inter-story shear force is still significant in the upper stories and the walls still surpass the linear limit for masonry walls. The shear force acting on the wall located above the springs is 519 kN, meaning that shear failure would be observed (because the shear strength is 0.38 MPa according to Meli and Reyes (1971) or 265 kN), which is a shortcoming of Model B.

### 3.3 Model C: Model B + compression strut in masonry walls (Record of SCT station)

The results of Model B show that the shear capacity is exceeded for all interior walls along the transverse direction. These three walls have the following characteristics: (a) a masonry wall located on Axis 3 properly confined by columns at both ends, (b) a wall on Axis 4 with a column at one end only, and (c) a wall along Axis 4a without confining elements. Therefore, for Model C, the wall along Axis 3 is assumed to be part of the seismic resisting system and is modeled as a nonlinear diagonal strut attached to the confining columns. In the absence of strong confining elements at both ends, the other two walls were modeled as shell elements with their elasticity modulus reduced by a factor of 0.25 to represent degraded stiffness. The loss of confinement effect of infills can be understood as a stiffness reduction observed in infill walls with openings (e.g., Dilmac 2020, Ozturkoglu *et al.* 2017). The recommendations proposed by Hwang *et al.* (2001)

were considered in modeling the Axis 3 masonry wall as a compression strut. The thickness of the strut corresponds to the thickness of the masonry wall, and the width of the strut was taken as equal to  $0.25l_w$ , where  $l_w$  is the diagonal length of the masonry, including the confinement columns.

Table 8 shows that the period of vibration in the transverse direction increased for Model C. Such behavior is to be expected, because the building becomes more flexible when the masonry walls are cracked. Fig. 13(d) shows that the seismic behavior in the longitudinal direction of the building is linearly elastic and that the Axis 3 diagonal strut displays a nonlinear response along the transverse direction. The peak compression force associated with the strut at Axis 3 is 697 kN (compressive strength 1360 kN). The shear forces of the walls at Elevations 4 and 4a, located in the elevator shaft (see Fig. 11) are 189 kN and 75 kN, respectively, giving shear stresses of 0.4 MPa and 0.15 MPa, respectively; therefore, the capacity of the Elevation 4 wall would be exceeded.

### *3.4 Model D: Model C + soil-foundation-structure interaction (Record of SCT station)*

Model D incorporates the effect of soil-foundation-structure interaction (SFSI) by joining the supports with rigid elements up to the geometric center of the foundation where springs and dashpots are included (Fig. 11(b)). Properties of the springs and dashpots are included in Table 7, for all 3 axial and all 3 rotation directions. Table 8 shows that the periods of vibration for Model D increase compared to those for Model C, mainly in the longitudinal direction. The increase in the period of vibration observed in the transverse direction is not significant because the springs on the second floor constrain the movement of the structure in that direction, so that the changes that occur above that floor are more relevant. Thus, the effect of SFSI is to change the structure to a significantly more flexible system in the longitudinal direction. The SFSI has no real effect on the behavior of the building in the transverse direction, because the constraint on the second floor minimizes the effects of ground motion. Fig. 12(e) shows that the seismic behavior of the building is linear and that the roof displacement in the longitudinal direction is two times higher than that in the previous cases. On the other hand, the seismic response in the transverse direction is slightly nonlinear.

The resultant total compression associated with the struts at Axis 3 is 762 kN. The shear force of the walls at Elevations 4 and 4a are 198 kN and 83 kN, respectively, which would result in shear stresses of 0.42 MPa and 0.16 MPa, respectively; that is, the capacity of the Elevation 4 wall would be exceeded. Thus, the shear stresses do not vary substantially when incorporating SFSI into the model, although it offers a better representation of the structure's natural period (Table 8).

### *3.5 Model E: Model D + partition masonry (Record of SCT station)*

Structures built in the 1950s commonly used partition elements to divide architectural spaces into different apartments. Such is the case for the Genova building, which has residential units on the third floor and above. In addition to the assumptions for Model D, Model E includes a thin masonry-type partition wall, which similar to typical infill walls can affect the building response (Aknouche *et al.* 2019, Demir and Cengiz 2021). The geometry of Model E is given in Fig. 10(e), which shows partitions between apartments at the entrances and some intermediate partitions. The partitions are modeled as masonry walls with a thickness of 7 cm, whose stiffness is 40% less than that of structural masonry walls. Due to the significant deformations that the building experienced

Table 9 Main stresses associated with the different models for SCT

Element	Parameter/Model	A <sup>1</sup>	B <sup>2</sup>	C <sup>3</sup>	D <sup>4</sup>	E <sup>5</sup>
Wall axis 3	$\sigma_{shear}$ [MPa]	0.85	0.74			
	$\sigma_{compression}$ [MPa]	-	-	3.42	3.74	2.94
	$\sigma_{shear strength}$ [MPa]	0.38	0.38			
	$f'_m$ [MPa]	6.8	6.8	6.8	6.8	6.8
Wall axis 4	$\Delta$ [mm]	8.3	5.2	8.0	9.5	6.8
	$\sigma$ [MPa]	0.67	0.66	0.40	0.42	0.32
	$\sigma_{shear strength}$ [MPa]	0.38	0.38	0.38	0.38	0.38
Wall axis 4a	$\sigma$ [MPa]	0.58	0.46	0.15	0.16	0.11
	$\sigma_{shear strength}$ [MPa]	0.38	0.38	0.38	0.38	0.38
	$V$ [kN]	56.6	27.2	45.6	64.5	29.8
Most demanded column	$N$ [kN]	519	19.4	1110	1204	928
	$M$ [kN m]	150	69	96	140	58
Most demanded beam	$V$ [kN]	98.4	43.1	34.9	38.1	24
	$M$ [kN m]	67	28	23	28	18

<sup>1</sup> N1 Column 3-C 20×60, N1 beam 4 B-C; <sup>2</sup> N2 Column 3-C 20×60, N2 beam 4 B-C; <sup>3</sup> N2 Column 3-C 20×50, N2 beam 4 B-C; <sup>4</sup> N2 Column 4-C 25×50, N2 beam 4 B-C; <sup>5</sup> N2 Column 4-C 20×50, N2 beam 4 B-C

during the earthquake, it is reasonable to expect these partitions to have contributed to the nonlinear behavior of the building. Table 8 shows that the Model E vibration periods are closer to those measured during the AVT (0.87 s and 0.58 s in the transverse and longitudinal directions, respectively).

Fig. 12(f) shows that the seismic behavior of Model E presents lower stresses compared to the previous models for Axis 3 and Axis 4. For the strut on Axis 3, the compressive force is 599 kN, while for Elevations 4 and 4a it is 150 kN and 56 kN, respectively, corresponding to stresses of 0.32 and 0.11 MPa, meaning that their strengths are not exceeded. When compared with Model D, Model E indicates that the shear stresses in the masonry infill walls decrease and stresses are distributed toward the partition masonry, which reaches a peak shear force of 82 kN in the transverse direction. The maximum shear strength of this partition masonry is calculated to be 87 kN, using the same resistance as the masonry infill walls, but accounting for a thickness of 7 cm and a length of 335 cm.

Table 9 summarizes the most important results for the stresses, forces, and displacements obtained from the five numerical models for the maximum shear in each case. The maximum acting shear and compressive stresses,  $\sigma$ , and the shear and compressive strengths,  $\sigma_{max}$ , of the key elements are included in the table. The inter-story displacement,  $\Delta$ , is also included to verify the corresponding limit state of the walls and compare it with both the observed behavior of the building and the limit states recommended in previous studies. The table shows that wall-type elements are susceptible to structural stiffness changes, affecting how the stress is redistributed towards the other elements. Any change resulting in an increase or decrease of stiffness will affect the period of vibration of the building and, consequently, the stresses produced by the inertial forces of the earthquake, which can vary substantially since the response in the flexible direction is within the first peak of the SCT record, which was used in Models A to E. On the other hand, the

shear ( $V$ ), moment ( $M$ ), and axial force ( $N$ ) presented by the columns may be wrong in Models A and B, because the walls did not experience shear failure in the actual building. When the masonry on Axis 3 is modeled as a compression strut (i.e., in Models C, D and E), the shear strength of the masonry wall increases due to its confinement by the surrounding frame. Finally, the contribution of the secondary elements in Model E is not negligible because it results in a reduction of the compressive stress of the wall on Axis 3 from 3.74 to 2.94 MPa.

#### 4. Conclusions

The response of a building in Mexico City that was not damaged structurally, despite having a configuration similar to those of damaged buildings, was assessed in this study. A suitable density of walls characterizes the studied building in the longitudinal direction (3.1%); the walls in that direction are properly confined by columns and RC beams. In contrast, the density of the walls in the transverse direction is low (0.8%), and there is just one wall properly confined, along elevation 3. Five 3D numerical models (Models A to E) were used in the study to model the seismic response of the building. Similar periods of vibration to those that were recorded were observed for Model D ( $T_{long} = 0.59$  s,  $T_{trans} = 0.96$  s) and Model E ( $T_{long} = 0.58$  s,  $T_{trans} = 0.87$  s), after incorporating the effect of adjacent buildings, modifying the Axis 3 wall as a compression strut together with a stiffness reduction in the walls on Axes 4 and 4a and incorporating soil-foundation-structure interaction. This suggests that once the linear behavior of the main resisting elements is exceeded, a force redistribution takes place between structural elements.

- Based on the evidence of pounding with adjacent buildings and considering that there are two-story buildings on both sides, all contiguous, it is evident that there was an interaction between buildings (Model B). However, the period of vibration for Model B, especially in the longitudinal direction (0.42 s), is still inconsistent compared to that obtained from AVTs (0.68 s). Considering a strut to model the masonry wall in Model C, the building becomes more flexible in the transverse direction ( $T_{trans} = 0.97$  s). More importantly, however, it drastically reduces the utilization factor to 0.5 ( $\sigma_{compression}/f_m'$ ) on the strut which is consistent with unobserved damage.

- Although the stresses in the walls were not significantly altered by incorporating the soil-foundation-structure interaction (Model D), the period of vibration increased in the longitudinal direction (0.59 s), reaching similar values to the AVT data. Due to the long periods and the deformations achieved, the non-structural elements (partitions) were incorporated (Model E), and they were found to have a material contribution to the building's behavior. Considering all of these factors, a behavior very close to what was recorded was achieved. The numerical results were compatible with the maximum stresses that are capable of being resisted by the building frames in the short direction and by the large walls in the longitudinal direction.

- In summary, key aspects were identified that are relevant to predict a reliable response for RC frame systems with masonry infill walls. The strut model and strength for masonry captured a larger capacity; the effect of soil-foundation-structure interaction in soft soil corrected the estimation of the system period in the flexible direction; the interaction with neighboring buildings, in this case with full contact on the sides, was relevant to redistribute forces along the height and modify the building period; and the impact of non-structural partitions on the stiffness and strength of frame buildings with infills was significant.

## Acknowledgments

The authors thank Professor Hector Guerrero from the Institute of Engineering at the National University of Mexico (UNAM) for providing drawings, results of ambient vibration tests and preliminary numerical models of the Genova 70 building. Julian Carrillo thanks Vicerrectoría de Investigaciones at Universidad Militar Nueva Granada for providing research grants.

## References

- Aknouche, H., Airouche, A. and Bechtoula, H. (2019), "Effect of masonry infilled panels on the seismic performance of a R/C frames", *Earthq. Struct.*, **16**(3), 329-348.  
<https://doi.org/10.12989/eas.2019.16.3.329>.
- Alcocer, S., Behrouzi, A., Brena, S., Elwood, K., Irfanoglu, A., Kreger, M., Lequesne, R., Mosqueda, G., Pujol, S., Puranam, A., Rodriguez, M. and Shah, P. (2020), "Observations about the seismic response of RC buildings in Mexico City", *Earthq. Spectra*, **36**(2\_suppl), 154-174.  
<https://doi.org/10.1177/8755293020942523>.
- Arteta, C.A., Carrillo, J., Archbold, J., Gaspar, D., Pajaro, C., Araujo, G., Torregroza, A., Bonett, R., Blandon, C., Fernandez- Sola, L., Correal, J. and Mosalam, K. (2019), "Response of midrise reinforced concrete frame buildings to 2017 Puebla earthquake", *Earthq. Spectra*, **35**(4), 1763-1793.  
<https://doi.org/10.1193/061218EQS144M>.
- Astroza, M., Moroni, O., Brzev, S. and Tanner, J. (2012), "Seismic performance of engineered masonry buildings in the 2010 Maule earthquake", *Earthq. Spectra*, **28**(1\_suppl1), 385-406.  
<https://doi.org/10.1193/1.4000040>.
- Bendat, J.S. and Piersol, A.G. (2011), Random Data: Analysis and Measurement Procedures, Fourth Edition, John Wiley & Sons, Hoboken, New Jersey, U.S.A.
- Bouarroudj, M.A. and Boudaoud, Z. (2022), "Numerical investigation of predicting the in-plane behavior of infilled frame with single diagonal strut models", *Struct. Eng. Mech.*, **81**(2), 131-146.  
<https://doi.org/10.12989/sem.2022.81.2.131>.
- Brincker, R., Zhang, L. and Andersen, P. (2001), "Modal identification of output-only systems using frequency domain decomposition", *Smart Mater. Struct.*, **10**(3), 441-445. <https://doi.org/10.1088/0964-1726/10/3/303>.
- CDMX Early Warning System (2017), Centro de Instrumentación y Registro Sísmico, A. C.; Center for Instrumentation and Seismic Registration (CIRES), Mexicocity, Mexico. <http://cires.org.mx>
- Chock, G., Robertson, I., Kriebel, D., Nistor, I., Francis, M., Cox, D. and Yim, S. (2011), "The Tohoku, Japan, Tsunami of March 11, 2011: Effects on Structures", EERI Special Earthquake Report, Earthquake Engineering Research Institute, Oakland, CA, U.S.A.
- Computers & Structures INC. (2004), *CSI Analysis Reference Manual for SAP2000, ETABS, SAFE and CSIBridge*, Structural & Earthquake Engineering Software, Walnut Creek, California, U.S.A.
- Demir, A. and Cengiz, M.M. (2021), "Effect of infill wall properties on seismic response of RC structures", *Comput. Concr.*, **27**(6), 513-521. <https://doi.org/10.12989/cac.2021.27.6.513>.
- Dilmac, H. (2020), "Influence of openings of infill wall on seismic vulnerability of existing RC structures", *Struct. Eng. Mech.*, **75**(2), 211-227. <https://doi.org/10.12989/sem.2020.75.2.211>.
- DOF CXXXIII (1942) State construction regulation 1942, Federal District Department; Guadalajara, Mexico.
- Federal District Government (2004), "Complementary Technical Standards", Volume II No. 103 BIS; Organ of the Government of the Federal District.
- Galvis, F., Miranda, E., Heresi, P., Dávalos, H., Silos, J.R. and Blume, J.A. (2017), "Preliminary Statistics of Collapsed Buildings in Mexico City in the September 19, 2017 Puebla-Morelos Earthquake", John A. Blume Earthquake Engineering Center and Department of Civil and Environmental Engineering, Stanford

- University, California, U.S.A.
- Galvis, F., Miranda, E., Heresi, P., Dávalos, H. and Ruiz-García, J. (2020), "Overview of collapsed buildings in Mexico City after the 19 September 2017 (Mw7.1)earthquake", *Earthq. Spectra*, **36**(2\_suppl), 83-109. <https://doi.org/10.1177/8755293020936694>.
- Gómez, A., Arellano, E., González, O. and Juárez, H. (2019), "Characteristics, causes, and consequences of the damages due to the earthquake of September 19, 2017 (M = 7.1) in Mexico", XII Chilean Conference of Seismology and Seismic Engineering, ACHISINA, Valdivia, Chile.
- Google Maps. (2019), Genova Building #70; retrieved September 5, 2019, Ciudad Juárez, Mexico. <https://maps.google.com>
- Guerrero, H. (2018), "Drawings, ambient vibration tests and preliminary numerical models of the Genova 70 building", Institute of Engineering, UNAM.
- Hashash, Y.M.A. (2016), "Nonlinear and equivalent linear seismic site response of one-dimensional soil columns", DEEPSOIL V.6.1; Department of Civil and Environmental Engineering, University of Illinois, Illinois, U.S.A.
- Hwang, S.J., Fang, W.H., Lee, H.J. and Yu, H.W. (2001), "Analytical model for predicting shear strength of squat walls", *J. Struct. Eng.*, **127**(1), 43-50. [https://doi.org/10.1061/\(ASCE\)0733-9445\(2001\)127:1\(43\)](https://doi.org/10.1061/(ASCE)0733-9445(2001)127:1(43))
- Jaime, A., Romo, M. and Ovando, E. (1987), "D-029 - Soil Characteristics at the SCT Site", Institute of Engineering, UNAM.
- Lan, Y.J., Stavridis, A., Kim, I., Diaz-Fanas, G., Heintz, J., Hernandez-Bassal, L., Anzola, E., Berkowitz, R., Hussain, S. and Jalalian, A. (2020), "ATC Mw7.1 Puebla-Morelos earthquake reconnaissance observations, Structural observations and instrumentation", *Earthq. Spectra*, **36**(2\_SUPPL), 31-48. <https://doi.org/10.1177/8755293020977520>.
- Lemnitzer A., Massone L.M., Skolnik D. A., Juan, C. and Wallace J.W. (2014), "Aftershock Response of RC Buildings in Santiago, Chile, succeeding the Magnitude 8.8 Maule Earthquake", *Eng. Struct.*, **76**, 324-338. <https://doi.org/10.1016/j.engstruct.2014.07.003>.
- Massone, L.M. and Cáceres, I. (2020), "Damage correlation in flexural walls with a displacement approach method for boundary detailing", *J. Build. Eng.*, **32**, 101807. <https://doi.org/10.1016/j.jobe.2020.101807>.
- Massone, L.M., Bedecarratz, E., Rojas F. and Lafontaine, M. (2021), "Nonlinear modeling of a damaged reinforced concrete building and design improvement behavior", *Journal of Building Engineering*, **41**, 102766. <https://doi.org/10.1016/j.jobe.2021.102766>.
- Meli, R. and Reyes, A. (1971), "Mechanical properties of masonry", Faculty of Engineering, UNAM.
- Mendoza, C.J. (1985), "Mechanical properties of concrete manufactured in the federal district", Engineering Institute, UNAM.
- NEHRP. (2012), "Soil-Structure Interaction for Building Structures. National Institute of Standards and Technology", NIST GCR 12-917-21; National Institute of Standards and Technology, Maryland, U.S.A.
- Ochoa-Cornejo, F., Pasten, C., Hernandez, F. and Astroza, R. (2019), "Geotechnical Aspects of the 2017 Mw 7.1 Puebla-Morelos Earthquake", XII Chilean Congress of Seismology and Seismic Engineering, ACHISINA, Valdivia, Chile, April.
- Ozturkoglu, O., Ucar, T. and Yesilce, Y. (2017), "Effect of masonry infill walls with openings on nonlinear response of reinforced concrete frames", *Earthq. Struct.*, **12**(3), 333-347. <https://doi.org/10.12989/eas.2017.12.3.333>.
- Public Administration of the Federal District, PAFD (2004), *Fourteenth Period, No. 103*, Official Gazette of the Federal District, October.
- Pujol, S. and Rodriguez, M.E. (2019), "Performance of non-structural elements in building in the earthquake of september 19, 2017 in Mexico City" (In Spanish), *Ingeniería sísmica*, **101**. <https://doi.org/10.18867/ris.101.529>
- Reinoso, E., Quinde, P., Buendia, L. and Ramos, S. (2021), "Intensity and damage statistics of the September 19, 2017 Mexico earthquake: Influence of soft story and corner asymmetry on the damage reported during the earthquake", *Earthq. Spectra*, **37**(3), 1875-1899. <https://doi.org/10.1177/8755293020981981>.
- Rodríguez, M. and Botero, J.C. (1996), "Aspects of the seismic behavior of reinforced concrete structures

- considering the mechanical properties of reinforcing steels produced in mexico”, Publicación Series of Engineering institute, UNAM.
- Tabeshpour, M.R. and Arasteh, A.M. (2019), “A new method for infill equivalent strut width”, *Struct. Eng. Mech.*, **69**(3), 257-268. <https://doi.org/10.12989/sem.2019.69.3.257>.
- Van Overschee, P. and De Moor, B. (1996), “Subspace Identification for Linear System: Theory - Implementation - Applications”, Kluwer Academic Publishers, Dordrecht, Netherlands.
- Working group of the National Seismological Service (WGNSS) (2017), “Special Report: Earthquake of September 19, 2017, Puebla-Morelos (M 7.1)”, UNAM.

TK